ChemPubSoc Europe

DOI: 10.1002/chem.201802757

CHEMISTRY A European Journal Full Paper

Computational Chemistry

Microfluidic Analyte Transport to Nanorods for Photonic and Electrochemical Sensing Applications

N. Scott Lynn, Jr. and Jiří Homola*[a]

Abstract: There has recently been a growing use of surface bound nanorods within electrochemical and optical sensing applications. Predictions of the microfluidic rate of analyte transport to such nanorods (either individual or to an array) remain important for sensor design and data analysis; however, such predictions are difficult, as nanorod aspect ratios can vary by several orders of magnitude. In this study, through the use of numerical simulation, we propose an explicit analytical approach to predict the steady-state diffusion-limited rate of mass transport to (individual) surface bound nanorods of variable aspect ratio. We show that, when compared to simulation, this approach provides accurate estimations across a wide range of Péclet numbers.

Introduction

Over the past decade, advancements in nanofabrication techniques have spawned a growing use of surface-bound nanoparticles for sensing purposes. Of these nanoparticles, gold nanorods have received a significant amount of attention for both optical[1] and electrochemical[2] applications, primarily due to their high surface-area-to-volume ratio, biocompatibility, and efficient mass transport characteristics. Although there have been a number of sensors based on the use of a single nanorod,[3] the majority of previous studies have used arrays of nanorods.[4]

We recently demonstrated that analyte transport to an array of NPs is dependent on the size and shape of the individual NPs composing the array.[5] This dependency becomes especially relevant for nanorod-based sensors, as the aspect ratio of individual nanorods (and thus rates of analyte interaction) can have orders of magnitude variations across different applications. Accurate prediction of rates of transport can greatly aid in both sensor design and optimization, as well as the analysis of experimental data.[6] Although modern numerical simulations can provide accurate predictions, they do so on a case-by-case basis. In contrast, the availability of an analytical solution for such predictions holds more power.

Solutions for steady-state diffusion-limited rates of transport have been found for a variety of surfaces pertinent to micro- and nanoparticle-based sensors. Analytical solutions derived from fundamentals often involve pure diffusive transport in infinite domains (void of convection) to simple shapes having convenient symmetry, including embedded disks and strips, hemispheres,[7] hemispheroids,[8] embedded rings,[9] ellipsoids,[10] sphere caps,[11] and hemitoroids.[12] Prediction of transport to more complicated shapes requires the use of numerical methods, where several approaches (e.g., finite difference, volume, element) have been used to simulate transport to (among others) embedded squares and bands,[13] cylinders,[14] cones,[15] and heptodes.[16] Results from simulation are often used to construct analytical approximations for rates of transport.

In this study, through the aid of numerical simulation, we propose a simple analytical approximation to predict the rate of transport to a single nanorod in a microfluidic flow cell having variable aspect ratio in both the vertical and horizontal direction. We consider several nanorod forms, as well as their derivatives, including nanocylinders and embedded nanobands, nanodisks, and nanosquares (Figure 1). We show that our approximation provides accurate prediction of transport to these shapes over a wide range of convective/diffusive conditions. Results from this study can be readily combined with the theory previously reported by Lynn and Homola[5] to predict steady-state rates of transport to arrays nanorods.

Motivation

Figure 1 shows a schematic of the problem and domain examined herein. We consider the transport of an analyte having inlet concentration c_o and diffusivity D within a fluidic channel

[a] Dr. N. S. Lynn, Jr., Prof. Dr. J. Homola
Institute of Photonics and Electronics
Czech Academy of Sciences
Chaberská 57, 18251 Prague (Czech Republic)
E-mail: homola@ufe.cz

The ORCID identification number(s) for the author(s) of this article can be found under:
https://doi.org/10.1002/chem.201802757.

Part of the Special Issue for the 7th EuCheMS Chemistry Congress consisting of contributions from selected speakers and conveners. To view the complete issue, visit Issue 46.

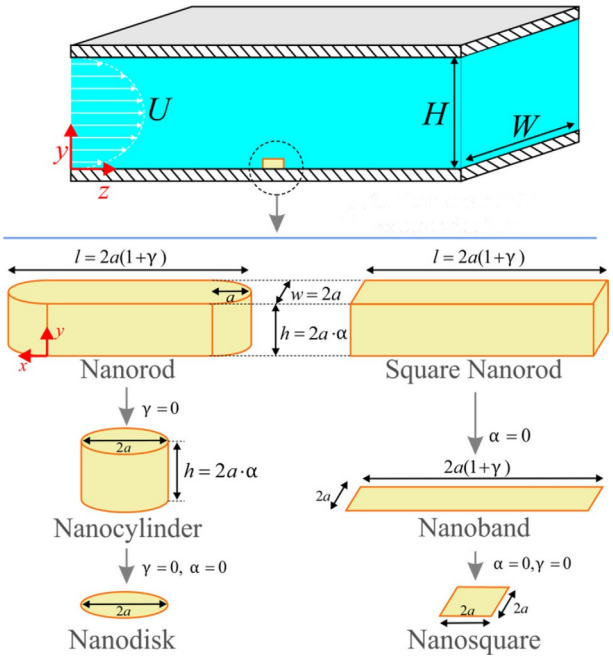

Figure 1. Schematic of the catalytic nanorods used in this study. Each nanoparticle has a surface area *A* (in contact with the fluid), and sits on the floor of a microchannel, far from the channel sidewalls.

having width *W* and height *H*. Flow through the channel has an average fluid velocity *U* and is considered to be laminar, with a Reynolds number $\mathrm{Re} = UH/\nu$, where ν is the kinematic viscosity of the fluid. A nanorod is situated on the floor of the microchannel, whose height and length can be characterized by two aspect ratios α and γ, respectively. We consider two similar shapes, one whose ends are rounded with a characteristic radius *a* (nanorod) and one with square ends (square nanorod). As seen in Figure 1, both shapes have derivatives that are commonly found within photonic and electrochemical applications, specifically, nanocylinders, nanobands, nanodisks, and nanosquares. The surfaces of the NP in contact with the fluid (characterized by a surface area *A*) are considered to be catalytically active, whereas all other channel surfaces are inert.

We consider the diffusion-limited transport of analyte to a nanorod surface, such that upon contact the analyte is instantaneously removed from the flow. Under such conditions the rate of analyte transport can be described by $\dot{N}$: the average rate of analyte interaction with the NP surface (molecules per time). For electrochemical applications this interaction would produce a current *i* such that $i = nF\dot{N}$, where *F* is the Faraday constant and *n* is the number of electrons exchanged. For nanorods capturing analyte via an affinity interaction (via an immobilized receptor), $\dot{N}$ describes the rate of analyte capture at the beginning of the assay.

The steady-state diffusion-limited rate of analyte interaction to a nanorod (or likewise, to any closed selectively active surface lying on an effective infinite planar support) can be described by Equation (1):

$$\dot{N}/c_o D = l_o \qquad (1)$$

where l_o is a characteristic length dependent on the geometry of the electrode. Relevant to this study, analytical solutions[7] for transport to a nanodisk lead to $l_o = 4a$, whereas numerical simulations for transport to a nanosquare[13] have led to $l_o = 4.606a$. These two values are valid for both diffusive transport in an infinite medium as well as mixed transport within a microchannel having a sufficiently small levels of fluid convection. The conditions for the latter can be described as $\mathrm{Pe}_{np} \ll 1$, where Pe_{np} is the nanoparticle Péclet number, which can be calculated using Equation (2):

$$\mathrm{Pe}_{np} = 6(l_o/4H)^2\mathrm{Pe} \qquad (2)$$

where $\mathrm{Pe} = UH/D$ is the channel Péclet number.

In this study, through the aid of computational simulation, we propose a function $f = f(\alpha, \gamma)$, such that the characteristic length for all of the NP shapes shown in Figure 1 can be described as $l_o = a \cdot f$. Knowledge of this parameter is important for several reasons, as it can be used to predict $\dot{N}$ [via Eq. (1)] for situations of diffusion dominated transport (i.e., $\mathrm{Pe}_{np} \ll 1$) and as we shall show later, for situations where convection plays a role.

Methods

We used the finite element package COMSOL to solve the Navier–Stokes (momentum) and convection-diffusion equations to obtain solutions for the velocity, pressure, and analyte concentration fields within a microfluidic domain. These solutions were used to calculate the rate of analyte transport to nanorods of varying shape and under varying conditions. Unless otherwise noted, the results herein concern transport to NPs having dimension of $a = 25$ nm within a microchannel of dimension $H = 100$ μm; nevertheless, similar results can be obtained using different dimensional values that are properly scaled to one another. The computational domain spanned the entire height of the channel (*y*-direction), and extended a distance of $150 \cdot l_o$ in both the upstream and downstream directions, as well as the same distance in the positive *x*-direction (taking advantage of symmetry). This domain was found to be large enough such that further increases in the domain size did not change any solution outcome (Figure 2).

For the momentum equations, we imposed a fully developed velocity profile at the domain inlet, a (pressure) outflow condition on the domain outlet, symmetric boundary conditions on both sidewall planes, and a no-slip condition on the top and bottom channel surfaces. For the convection-diffusion equations we imposed a constant analyte concentration (c_o) at the domain inlet and a no-flux condition along all other surfaces, where the concentration of analyte along the active NP surface was set to zero (in accordance with a diffusion-limited transport condition).

The mesh for each simulation was composed of tetrahedral elements, discretized linearly and quadratically for the momentum and convection-diffusion equations, respectively. The characteristic mesh size was variable within the domain, where the maximum size along nanorod edges was *a*/500 (the upper edge for nanorods with $\alpha > 0$), the maximum size in the volume immediate to (and along the surface of) each nanorod was *a*/10, and the maximum size in the far field regions was *H*/20. Mesh growth rates along and near each nanorod were set to 1.4, whereas in other regions growth rates were set to 1.1. Figure 2 shows a typical mesh along

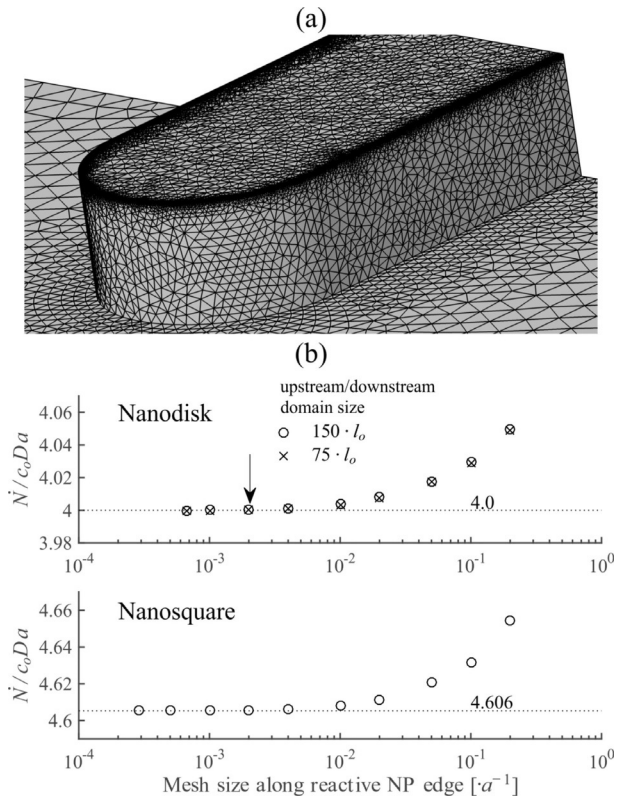

Figure 2. (a) Typical mesh for a nanorod ($\alpha = 0.5$, $\gamma = 2.7$) with a mesh size of $a/500$ along the upper nanorod edges. (b) Mesh density test for nanodisks and nanosquares as a function of the mesh size along the edge of each shape (independence of domain size shown in the nanodisk data). The converged values of 4.0 and 4.606 correspond to previous solutions for a nanodisk[7] and a nanosquare,[13] respectively. The arrow indicates the mesh density used within this study.

the surface of a nanorod, along with results from a mesh density test for both nanodisks and nanosquares (α, $\gamma = 0$). Additional mesh density tests for other selected nanorod shapes yielded similar convergence properties (data not shown). Reductions in either the mesh size or growth rate below these values was found to have only a minimal effect on the simulation outcomes. Average simulations consisted of $\approx 5 \times 10^6$ elements, dependent on the specific NP. Steady-state solutions were obtained using a multigrid method, using the successive over relaxation method for the pre- and post-smoother and the PARADISO method for the course solver. After convergence of each solution, steady values of the analyte interaction rate were calculated as $\dot{N} = \int \hat{n} \cdot (D\nabla c) dA$, where $\hat{n}$ is the normal vector for each nanorod reactive surface in contact with the fluid.

Results

For mesh verification we simulated analyte transport to both nanodisks and nanosquares. Figure 2b shows the results of these simulations, where data are plotted in a dimensionless form as $\dot{N}/c_oDa$.[1] At a mesh density of $a/500$ (along the edge of each NP) our simulation results were within 0.05% of standard solutions for nanodisks (4.0) and nanosquares (4.606).

[1] *The value* $\mathrm{Nu} = \dot{N}/c_oDa$ *is a dimensionless number known in mass (or heat) transfer as the Sherwood (or Nusselt) number.*

These two values thus form the base solution for transport to the derived shapes shown in Figure 1 as in Equation (3):

$$f_0 = \begin{cases} 4.0 & \text{for nanorod shapes,} \\ 4.606 & \text{for sqare nanorod shapes.} \end{cases} \quad (3)$$

We simulated transport to both nanocylinders and square posts (i.e., nanosquares with $\alpha > 0$) having variable vertical aspect ratio ($0 < \alpha < 25$) at low Péclet number. Figure 3 shows the results of these simulations. From the steady-state contour profiles, it can be seen that the overall size of the boundary layer increases with increases in α. This growth occurs in a complex fashion, where at high aspect ratios the shape of each boundary layer takes on a cylindrical form. The shape of these boundary layers lead to an edge effect phenomenon, leading to enhanced rates of transport near nanocylinder tops or similarly, nanorod caps (discussed later).

Despite the complexity in the shape of the boundary layer, the rate of analyte interaction follows a fairly simple trend. This is shown in Figure 3b, which plots data taken from finite element (FE) simulations regarding nanocylinders and square posts. We also plot numerical data previously given by Britz et al.[14b] It can be seen that all of the data has a very good match to the function $f_1 = f_0 + 6\alpha^{3/4}$. It should be noted that this function was chosen for its simplicity and accuracy and

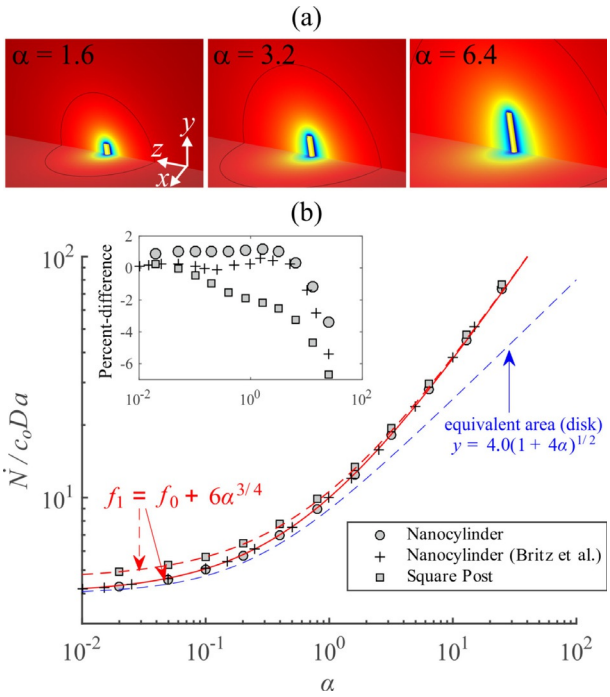

Figure 3. Mass transport to nanocylinders and square posts with variable vertical aspect ratio α ($\mathrm{Pe}_{np} = 10^{-5}$). (a) Steady-state analyte contours for nanocylinders along the channel floor (x,z plane) and the symmetry (y,z) plane. Flow is in the z-direction. The thin black line plots the analyte boundary layer ($c/c_o = 0.9$). (b) The rate of analyte interaction, normalized as $\dot{N}/c_oDa$, plotted as a function of α. We also include numerical data taken directly from Britz et al.[14b] The inset plots the percent difference between the numerical data and the function $f_1 = f_0 + 6\alpha^{3/4}$. The dashed blue line indicates predictions based on an equivalent surface area approach.

was not derived from first principles. The difference between values calculated via f_1 and data taken from FE simulations is less than 6% for the range of $0<\alpha<25$. Figure 3 also shows the predictions via an equivalent area approach, where transport to a 3D cylinder is estimated by the transport to a disk of equivalent surface area. It can be seen that as α increases, there is a large deviation between the numerical data and those predicted via such an approach.

We next simulated transport to nanobands having variable horizontal aspect ratio ($0<\gamma<400$). Figure 4 shows the results of these simulations. Data from FE simulations were observed to scale as $\propto\gamma^{17/20}$ at high aspect ratio. This trend was also observed for larger domains (100× larger a/H ratio), indicating the size of the domain had no influence on this scaling relationship. This relationship was also observed to hold for nanobands having $\gamma<10^4$ via simulations with lower density meshes (size of $a/20$ along the reactive edge, data not shown). The data from FE simulations were within 2% of the function $f_0+2.157\gamma^{17/20}$ (inset). Our results agree with those of Cutress and Compton[13] at low γ; however, at larger aspect ratios ($\gamma>10^2$) we observed a deviation from their proposed solution (which scales as $\propto\gamma$). Figure 4 also shows predictions via an equivalent area approach. As with the data in Figure 3, there is a large deviation from numerical data as γ increases.

Applying a similar approach to more complex shapes, we simulated analyte transport to nanorods and square nanorods having variable aspect ratios in the range of $0<\alpha<8$ and $0<\gamma<100$ at low Péclet number ($Pe_{np}=10^{-5}$); this range of nanorod sizes reflect those often used in experiment. Figure 5 shows the results of these simulations. As expected, there is an increase in the rate of analyte interaction with increases in both α and γ. Similar to the data in Figure 4, all of the data shown in Figure 5 asymptotically approach the scaling relationship $\dot{N}\propto\gamma^{17/20}$ in the range such that a nanorod length is much larger than its height ($\gamma\gg\alpha$). Using this data, we searched for a function f_2 in the form of $f_2=f_1+\Omega\gamma^{17/20}$, where $\Omega=\Omega(\alpha)$. The best fit for Ω resulted in $f_2=f_1+(2.157+0.525\alpha^{3/5})\gamma^{17/20}$. From data shown in the inset, it can be seen that all of the data from FE simulations are within 11% of those calculated via f_2. From this data, it follows that a fairly simple form of the characteristic length for catalytic nanorods can be expressed as Equation (4):

$$l_o/a=f_0+6\alpha^{3/4}+(2.157+0.525\alpha^{3/5})\gamma^{17/20} \quad (4)$$

which is written in the form of $l_o/a=f_0+f_2$, where f_0 is taken from Equation (3).

To test the merit of Equation (4) over a wider range of conditions, we simulated the analyte transport to nanocylinders ($0<\alpha<16$) and nanorods ($\alpha=2$, $2<\gamma<64$) of variable aspect ratio under conditions pertaining to the range $10^{-3}<Pe_{np}<10^3$. For a given nanoparticle shape, this range of Pe_{np} is often encountered experimentally via changes in U, H, or D (among other parameters). Figure 6 plots the data from these simulations, in the dimensionless form of $4\dot{N}/c_oDl_o$, as a function of Pe_{np}. We compare the FE simulation data with analytical solutions for transport to a nanodisk (Figure 6, red line). Specifically, we plot the solution given by both Phillips[17] as well as a modified[5] solution of that given by Stone[18] for low and high Péclet number flow, respectively. These solutions are rewritten here as Equation (5):

$$Nu_d=\begin{cases}\left(4-0.123Pe_{np}^{3/2}\right)\left(1-0.203Pe_{np}^{1/2}\right)^{-1} & (Pe_{np}<0.44)\\ 2.16Pe_{np}^{1/3}+4.04Pe_{np}^{-1/6}-1.29Pe_{np}^{-1/3} & (Pe_{np}>0.44)\end{cases} \quad (5)$$

For transport to a nanodisk, these solutions can be calculated as $Nu_d=\dot{N}/c_oDa$.

It can be seen that plotted in this manner, all of the data taken from FE simulations have a close match to the analytical solutions for transport to a nanodisk. For nanocyliders under conditions such that $Pe_{np}<1$, numerical data were within 5% of those calculated via Equation (5). For nanorods the differen-

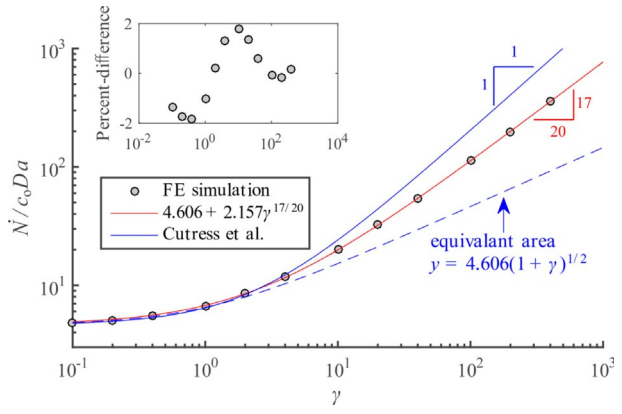

Figure 4. Mass transport to nanobands with variable horizontal aspect ratio γ ($Pe_{np}=10^{-5}$). The inset plots the percent difference between the numerical data and the function $4.606+2.157\gamma^{17/20}$ (solid red line). The dashed line plots the solution proposed by Cutress and Compton,[13] modified here to the form $\dot{N}/c_oDa=2(1+\gamma)(1.004+1.3\exp(-2.53\log_{10}(1+\gamma)))$. The dashed blue line indicates predictions based on an equivalent surface area approach.

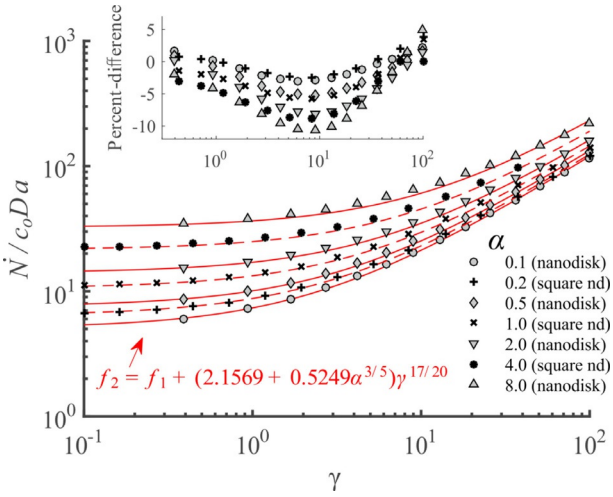

Figure 5. Mass transport to nanorods and square nanorods with variable aspect ratios in the vertical (α) and horizontal (γ) directions ($Pe_{np}=10^{-5}$). Data from FE simulations is plotted as symbols, and predictions (f_2) are shown in the red lines, solid for nanorods, dashed for square nanorods. The inset plots the percent difference between the FE simulation data and the function $f_2=f_1+(2.157+0525\alpha^{3/5})\gamma^{17/20}$.

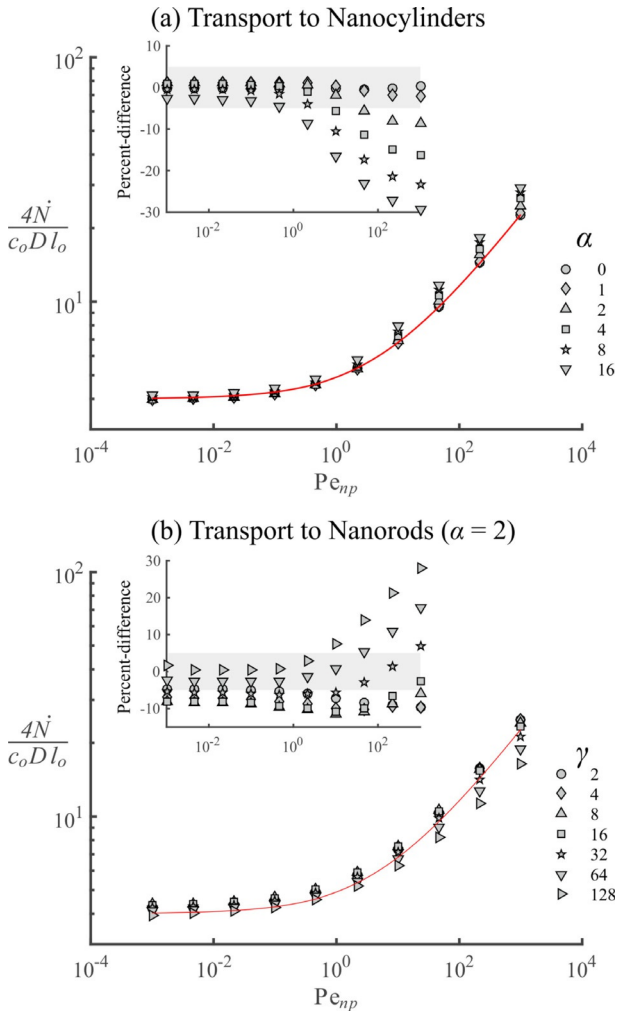

Figure 6. Transport to nanocylinders (a) and nanorods (b) having variable aspect ratio under variable Péclet number. For all data, $\dot{N}$ was taken from FE simulations and l_o was calculated via Equation (4). Simulations were carried out via variation of U (constant H, D). The inset shows the percent difference between data taken from FE simulations and that calculated by Equation (5) (plotted as a solid red line); the shaded region represents a difference of ±5%.

ces between numerical and analytical solutions were slightly larger: in the range of $Pe_{np}<1$ all differences were within 10%, whereas at for $Pe_{np}>1$ those differences were within 20%. Further simulations regarding nanorods with different vertical aspect ratios ($\alpha=1,4$) followed similar trends (data not shown).

Discussion

Application to experiment. The results in this study pertain to steady-state rates of analyte transport. It is important to know when these steady rates will be applicable to an experimental system. For low Péclet number applications, the transient rate of transport can be estimated as $\dot{N}/c_oD = l_o(1 + l_o/(4\pi^3 Dt)^{1/2})$.[9] Thus the characteristic time for transport to reach steady state (t_c) can be calculated as $t_c \approx l_o^2/4\pi^3 D$. For transport to nanoparticles these times can be very short, for example, a nanorod having $a=25$ nm with $\gamma=100$ and $\alpha=1$ will reach steady state at $t_c \approx 0.01$ s.

Low Pe_{np} transport to nanocylinders and nanobands. According to theory, the rate of analyte interaction for transport to nanocylinders (Figure 3) should scale as $\dot{N} \propto \alpha$ for situations when $\alpha \to \infty$. Such behavior was found by Britz et al.,[14b] who proposed a solution of $\dot{N}/c_oDa = 4 + 0.335\alpha^{1.152} + 5.603\alpha^{0.722}$ (modified to fit the geometry here), which begins to approximately scale as $\dot{N} \propto \alpha$ for cylinders with $\alpha > 10^2$. Within the range of aspect ratios shown in Figure 3, which represents the capability of modern fabrication techniques, their solution provides similar accuracy with respect to the one proposed herein.

A similar theoretical argument can be made for the nanobands, which should scale as $\dot{N} \propto \gamma$ for situations when $\gamma \to \infty$. Such scaling was found by Cutress and Compton.[13] We did not observe this scaling relationship under the range of parameters studied herein; all of our computational simulations yielded results similar to that shown in Figure 4 (which included variation in domain size, variation in mesh, and variation in solution method), where at large aspect ratio in the range of $\gamma < 400$ (up to $\gamma < 10^3$ for low quality meshes), the rate of analyte interaction scales as $\dot{N} \propto \gamma^{17/20}$. We were unable to perform simulations (even with low density meshes) above an aspect ratio of $\gamma > 10^4$, as such structures become computationally difficult to simulate.

One source of discrepancy between our results and those of Cutress and Compton, shown in Figure 4, can likely be attributed to the methodology they used for predicting steady-state responses. Specifically, they simulated the transient transport to variable aspect ratio nanobands, where simulation times were restricted to values corresponding to a dimensionless time of $\tau < 30$, where τ was defined (modified for the parameters used here) as $\tau = Dt/4a^2$. Predictions for the steady-state response were then obtained from fits to transient data; however, for these simulation times, transport to high aspect ratio nanobands were not observed to reach a full steady-state. To quantify this effect, we note that the dimensional characteristic time for transport to reach steady state ($t_c \approx l_o^2/4\pi^3 D$, defined above) leads to a dimensionless characteristic time of $\tau_c = 1/4\pi^3 \cdot (l_o/a)^2$. For the high aspect ratio nanobands in their study ($\gamma \approx 1000$), this leads to a value of $\tau_c \approx 1200$, much higher than the simulation times used in their study.

Prediction of analyte transport to single nanorods. The agreement between FE simulation data and the solutions for transport to a nanodisk (Figure 6) indicates that both the choice of l_o [Eq. (4)] and the calculation of Pe_{np} [Eq. (2)]are appropriate. This agreement thus serves as a simple route for prediction, where the steady-state rate of analyte interaction for a single nanorod can be calculated as in Equation (6):

$$\dot{N} = Nu_d \cdot c_o D l_o/4 \quad (6)$$

where Pe_{np}, l_o, and Nu_d can be calculated via Equation (2), (4), and (5), respectively. As seen in Figure 6, this method should enable predictions to single nanorods of varying shapes over a wide range of Péclet numbers with an accuracy of <10% for most experimental systems ($Pe_{np}<1$). The alignment of the nanorod with respect to the flow direction will have little to

no effect on $\dot{N}$ for conditions such that $Pe_{np} < 1$; we did not examine other nanorod alignments.

Prediction of analyte transport to arrays of nanorods. For applications involving arrays of nanorods, Equation (6) can be used with the results of our previous study.[5] Nevertheless, the results shown herein are directly useful for experiments based on nanorod arrays: the rate of transport to a single nanorod, measured in terms of analyte flux (rate of transport divided by active surface area) will define the upper limit for the flux to a surface composed of an array of such nanorods.

Prediction of spatially dependent transport to a single nanorod. In addition to predicting the rate of analyte interaction for the entire nanorod, the results given here can also be used to estimate the rate of collection by portions of the nanorod of interest. This is especially relevant for photonic applications, where electromagnetic fields are enhanced near the nanorod caps. The ratio between the rate of interaction by the caps of a nanorod ($\dot{N}_{cap}$, extending a distance a from each end) and that of the entire nanorod can be estimated as the ratio between the transport to a cylinder lying by itself (described by f_1) and that to the entire nanorod (described by f_2). The rate of interaction to the nanorod caps will monotonically decrease with increases in γ (influenced by the boundary layer along the sides of the nanorod), thus the ratio f_1/f_2 will provide an upper bound for $\dot{N}_{cap}/\dot{N}$. Figure 7 demonstrates this effect pertaining to a square nanorod with variable γ. Following the same line of reasoning, the ratio f_0/f_1 will provide an upper bound to the ratio between the rate of interaction by the upper face of a nanocylinder and the entire nanocylinder.

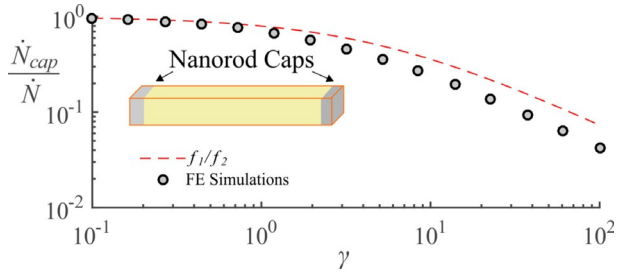

Figure 7. Ratio of the rate of interaction between the caps of a square nanorod ($\dot{N}_{cap}$ vs. the rate of interaction of the entire nanorod ($\dot{N}$). The caps of a nanorod extend a distance a from each end (shown as shaded grey in the schematic). All data pertains to a square nanorod with $\alpha = 1$ at $Pe_{np} = 10^{-5}$. The dashed line represents the function f_1/f_2.

Conclusions

In this study, we used numerical simulation to calculate the steady-state diffusion-limited rate of analyte transport nanorods lying on the surface of a fluidic channel. We considered a number of nanorod shapes as well their derivatives (Figure 1), all of which have importance within electrochemical and photonic applications. Based on the results of these simulations, we have proposed a simple analytical approximation to predict the rate of analyte transport to nanorods of variable aspect ratio, both in the horizontal and vertical direction. Our proposed solution, given by Equation (6), predicts rates of analyte interaction within 10% of results from numerical simulation at flows having low Péclet number (Figure 5); these predictions also maintain accuracy for flows of intermediate and high Péclet number (Figure 6). These results can also be applied to estimate the rate of analyte transport to the nanorod caps (Figure 7). The results of this study are useful for applications based on the use of a single nanorod as well as applications based on arrays of nanorods.

Acknowledgements

This work was supported by both the Praemium Academiae of the Academy of Sciences of the Czech Republic, the Czech Science Foundation (contract no. GBP205/12/G118), and the European Union's Horizon 2020 research and innovation program (project ULTRAPLACAD, contract no. 633937).

Conflict of interest

The authors declare no conflict of interest.

Keywords: biosensors · electrochemistry · microfluidics · nanoparticles · surface plasmon resonance

[1] a) J. Cao, T. Sun, K. T. Grattan, *Sens. Actuators B* **2014**, *195*, 332–351; b) I. Mannelli, M.-P. Marco, *Anal. Bioanal. Chem.* **2010**, *398*, 2451–2469.
[2] a) M. Alagiri, P. Rameshkumar, A. Pandikumar, *Microchim. Acta* **2017**, *184*, 3069–3092; b) P. A. Rasheed, N. Sandhyarani, *Microchim. Acta* **2017**, *184*, 981–1000.
[3] a) G. J. Nusz, S. M. Marinakos, A. C. Curry, A. Dahlin, F. Höök, A. Wax, A. Chilkoti, *Anal. Chem.* **2008**, *80*, 984–989; b) P. Zijlstra, P. M. Paulo, M. Orrit, *Nat. Nanotechnol.* **2012**, *7*, 379; c) I. Ament, J. Prasad, A. Henkel, S. Schmachtel, C. Sönnichsen, *Nano Lett.* **2012**, *12*, 1092–1095.
[4] a) M. Ongaro, P. Ugo, *Anal. Bioanal. Chem.* **2013**, *405*, 3715–3729; b) B. Špačková, P. Wrobel, M. Bocková, J. Homola, *Proc. IEEE* **2016**, *104*, 2380–2408.
[5] N. S. Lynn, Jr., J. I. Homola, *Anal. Chem.* **2016**, *88*, 12145–12151.
[6] B. Špačková, N. S. Lynn, Jr., J. I. Slabý, H. Šípová, J. Homola, *ACS Photonics* **2018**, *5*, 1019–1025.
[7] K. Aoki, *Electroanalysis* **1993**, *5*, 627–639.
[8] J. C. Myland, K. B. Oldham, *J. Electroanal. Chem. Interfacial Electrochem.* **1990**, *288*, 1–14.
[9] A. Szabo, *J. Phys. Chem.* **1987**, *91*, 3108–3111.
[10] S. Bruckenstein, J. Janiszewska, *J. Electroanal. Chem.* **2002**, *538*, 3–12.
[11] L. R. Alfred, K. B. Oldham, *J. Phys. Chem.* **1996**, *100*, 2170–2177.
[12] L. R. Alfred, J. C. Myland, K. B. Oldham, *J. Electroanal. Chem. Interfacial Electrochem.* **1990**, *280*, 1–25.
[13] I. J. Cutress, R. G. Compton, *J. Electroanal. Chem.* **2010**, *645*, 159–166.
[14] a) E. J. Dickinson, I. Streeter, R. G. Compton, *J. Phys. Chem. C* **2008**, *112*, 11637–11644; b) D. Britz, O. Østerby, J. Strutwolf, *Electrochim. Acta* **2010**, *55*, 5629–5635; c) R. Ferrigno, P. Brevet, H. Girault, *Electrochim. acta* **1997**, *42*, 1895–1903.
[15] C. G. Zoski, M. V. Mirkin, *Anal. Chem.* **2002**, *74*, 1986–1992.
[16] O. Sklyar, J. Ufheil, J. Heinze, G. Wittstock, *Electrochim. Acta* **2003**, *49*, 117–128.
[17] C. G. Phillips, *Q. J. Mech. Appl. Math.* **1990**, *43*, 135–159.
[18] H. A. Stone, *Phys. Fluids A* **1989**, *1*, 1112–1122.

Manuscript received: June 1, 2018
Revised manuscript received: July 13, 2018
Accepted manuscript online: July 20, 2018
Version of record online: July 25, 2018

